Thyroid Gland Tumor Diagnosis at US Elastography[1]

Andrej Lyshchik, MD
Tatsuya Higashi, MD, PhD
Ryo Asato, MD, PhD
Shinzo Tanaka, MD, PhD
Juichi Ito, MD, PhD
Jerome J. Mai, MSc
Claire Pellot-Barakat, PhD
Michael F. Insana, PhD
Aaron B. Brill, MD, PhD
Tsuneo Saga, MD, PhD
Masahiro Hiraoka, MD, PhD
Kaori Togashi, MD, PhD

Published online before print
10.1148/radiol.2363041248
Radiology 2005; 237:202–211

Abbreviation:
RF = radiofrequency

[1] From the Departments of Nuclear Medicine and Diagnostic Imaging (A.L., T.H., T.S., K.T.), Otolaryngology-Head and Neck Surgery (R.A., S.T., J.I.), and Therapeutic Radiology and Oncology (M.H.), Kyoto University Graduate School of Medicine, Sakyo-ku, Kyoto 606-8507, Japan; Department of Biomedical Engineering, University of California, Davis, Davis, Calif (J.J.M., C.P., M.F.I.); and Department of Radiology and Radiological Sciences, Vanderbilt University, Nashville, Tenn (A.B.B.). Received July 16, 2004; revision requested September 27; revision received October 8; accepted November 15. Supported in part by NSF award 9817722. **Address correspondence to** A.L. (e-mail: *lyshchik@kuhp.kyoto-u.ac.jp*).

Authors stated no financial relationship to disclose.

Author contributions:
Guarantors of integrity of entire study, A.L., T.H.; study concepts/study design or data acquisition or data analysis/interpretation, all authors; manuscript drafting or manuscript revision for important intellectual content, all authors; approval of final version of submitted manuscript, all authors; literature research, A.L.; clinical studies, A.L., T.H., R.A., S.T.; experimental studies, A.L., J.J.M., C.P.; statistical analysis, A.L.; manuscript editing, A.L., T.H., J.J.M., C.P., M.F.I., A.B.B., T.S.

PURPOSE: To prospectively evaluate the elastographic appearance of thyroid gland tumors and explore the potential sensitivity and specificity of ultrasonographic (US) elastography for differentiating benign and malignant tumors, with histopathologic analysis as the reference standard.

MATERIALS AND METHODS: The study was institutional review board approved, and each patient gave written informed consent. Fifty-two thyroid gland lesions (22 malignant, 30 benign) in 31 consecutive patients (six men, 25 women; mean age, 49.7 years ± 14.7 [standard deviation]) were examined with real-time elastography in the elasticity imaging mode implemented on a clinical US scanner modified for research. In addition, the radiofrequency echo data stored during US were exported from the scanner and used for off-line strain image reconstruction. All elastograms were evaluated for the lesion visibility, relative brightness, and margin regularity and definition by using a four-point scale. In addition, normal thyroid gland tissue and thyroid gland tumor strains were measured on off-line processed elastograms, and the thyroid gland–to-tumor strain ratio (ie, strain index) was calculated. The potential of elastographic criteria for the diagnosis of thyroid gland cancer was evaluated with univariate analysis and multivariate logistic regression. Qualitative variables were compared by using the χ^2 test, and quantitative variables were compared by using the Mann-Whitney *U* test. $P < .05$ was considered to indicate significance.

RESULTS: A strain index value greater than 4 on off-line processed elastograms was the strongest independent predictor of thyroid gland malignancy ($P < .001$); this criterion had 96% specificity and 82% sensitivity. Two other elastographic criteria, which were evaluated on real-time elastograms—a margin regularity score higher than 3 (88% specificity, 36% sensitivity) and a tumor area ratio higher than 1 (92% specificity, 46% sensitivity)—also were associated with malignancy ($P < .05$). However, the usefulness of these criteria was not considered to be high because of their low sensitivity.

CONCLUSION: Elastography is a promising imaging technique that can assist in the differential diagnosis of thyroid cancer.

Palpation is the oldest and most frequently used screening method for detecting thyroid gland tumors. In general, almost 5% of the adult population have a palpable thyroid gland nodule. Furthermore, with ultrasonographic (US) screening of clinically normal thyroid glands, one or more thyroid gland nodules can be detected in about 50% of patients, particularly those older than 50 years (1–3). Although most thyroid gland nodules are benign, the possibility of cancer must always be considered. One of the key features of thyroid gland cancer evaluated at palpation is the degree of firmness: Malignant lesions tend to be much harder than benign ones (4). Unfortunately, palpation is a highly subjective method and is dependent on the size and location of the nodule and on the skill of the practitioner (5). US examination is a very accurate and highly sensitive method for detecting thyroid gland lesions; however, its usefulness in differentiating between benign and malignant thyroid gland tumors is relatively low (6). For patients with thyroid gland nodules, fine-needle aspiration biopsy has proved to be an efficient tool for thyroid cancer diagnosis. Despite the advantages of fine-needle aspiration biopsy, it is an invasive procedure and subject to sampling and analysis uncertainties. Thus, improved, more reliable criteria for determining which nodules should be followed up and which should be aspirated are needed (7).

The diagnostic advantages of high-frequency US examination and the accuracy of thyroid cancer diagnosis based on the lesion's stiffness are combined in US elastography (8,9). Although US elastography is not yet used in routine clinical practice, it has been shown to be useful in the differential diagnosis of breast and prostate cancers (10,11). Of all the elastographic techniques, tissue strain imaging under a quasistatic compression load is the simplest to use and is very promising (12). With this method, strain images are constructed by using measurements of the local displacements induced by a compressive force applied to the tissue surface. The displacement fields are estimated by using correlation techniques that track the echo delays in segmented waveforms that are recorded before and after the quasistatic compression (13). The results of the tissue compression are displayed as an image called an elastogram, on which hard areas appear dark and soft areas appear bright. Currently, there are two approaches to this method: The first approach involves the use of two-dimensional correlation-based speckle trackers to produce real-time (7 frames per second) elastograms along with a B-mode sonogram in spatial and temporal registration. With the second approach, the radiofrequency (RF) data are recorded and stored for off-line elastogram formation. The off-line image reconstruction algorithms involve the use of a series of speckle-tracking approaches to estimate the local deformation from coarse to fine spatial scales. This technique yields images that have higher spatial and contrast resolution and lower motion sensitivity and strain noise but no temporal information.

The thyroid gland is well positioned for elastographic examination: It is easily assessable and can be efficiently compressed against underlying anatomic structures by using a US probe. The aim of our prospective study was to evaluate the elastographic appearances of thyroid gland tumors and to explore the sensitivity and specificity of US elastography for differential diagnosis of thyroid cancer, with histopathologic analysis as a reference standard.

MATERIALS AND METHODS

To perform this study, both a kit to modify the Sonoline Elegra US scanner (Siemens Medical Systems, Issaquah, Wash) for research and a mechanical analyzer (EZ-Test; Shimadzu, Kyoto, Japan) were loaned to us from the manufacturers (Siemens Medical Systems and Shimadzu, respectively). We had full control over the data and the information that were submitted for publication.

Patients

Fifty-two consecutive thyroid gland tumors in 31 patients who were referred for consideration of surgical treatment were examined in this prospective study. The study was conducted during a 6-month period from January to June 2004. The study protocol was approved by the institutional review board of Kyoto University. Before enrollment, each patient gave written informed consent, as required by the Kyoto University human study committee.

The mean age of the examined patients—six men and 25 women—was 49.7 years ± 14.7 (standard deviation) (age range, 25–74 years). All patients had normal serum levels of thyroid and thyroid-stimulating hormones. All except one patient underwent surgery, and the final diagnosis was based on the results of histopathologic examination of resected thyroid gland tissue. One 67-year-old female patient with four apparently benign thyroid gland tumors (two solid, two cystic) declined to undergo surgery. The diagnosis in this case was based on cytologic, clinical, and US findings. Twenty (38%) lesions were diagnosed as papillary thyroid carcinoma; two (4%) lesions, as follicular carcinoma; 15 (29%) lesions, as follicular adenoma; and 15 (29%) lesions, as adenomatous goiter. Twelve (39%, all female) patients had multiple thyroid gland lesions: Three patients had multiple malignant nodules; four, multiple benign nodules; and five, multiple benign and malignant lesions.

US Examinations

In all patients, US was performed by using a clinical scanner (Sonoline Elegra) that was modified for research and a 7.5-MHz linear probe (Siemens Medical Systems). The US images were acquired, reviewed, and interpreted by two radiologists (A.L., T.H.) who were blinded to the patients' final diagnoses. Before the study, the radiologists agreed on the methods of image acquisition and interpretation. Decisions regarding the findings were reached by consensus. The first investigator (A.L.) had 6 years of experience performing diagnostic US of the thyroid gland, and the second investigator (T.H.) had 15 years of this experience.

For all patients, the US examination started with B-mode imaging. The positioning of the patients for imaging was identical to that used for standard clinical thyroid gland US: The patient was positioned on his or her back with the neck slightly extended over a pillow. During B-mode US, thyroid gland lesions were identified and a region of interest for elastography was identified. The size of B-mode images was 40 mm in depth and 40 mm in lateral width; the size of the region of interest for elastography was 35 mm in depth and 30 mm in lateral width.

Real-time US Elastography in Elasticity Imaging Mode

After B-mode US, real-time strain imaging in the elasticity imaging mode that was implemented on the US scanner modified for research was performed for each region of interest that was selected during B-mode US. With use of the US probe, light compression was applied to the anterior neck above the examined lesion to fix the position of the thyroid gland and limit its lateral movement. Then, light compression was applied to the same area again. During the second compression, the B-mode sonogram and strain image formed from the same RF data were displayed side-by-side on the screen to aid in lesion identification. The real-time elastograms were acquired at 7 frames per second.

For each lesion examined, a total of 91 strain images that were acquired during three compression-relaxation cycles were stored in the cine-buffer memory of the US scanner. We then selected the three best fit B mode sonogram–elastogram image pairs and evaluated them for the lesion visibility, relative brightness, and margin regularity and definition by using a four-point scale (Table 1). The depth *(D)* and width *(W)* of each lesion on the B-mode sonograms and real-time elastograms were calculated. The area *(A)* of the lesion depicted on the B-mode sonogram and that depicted on the real-time elastogram were calculated separately, with the assumption that the lesion had an elliptical shape, as follows: $A = (D/2) \cdot (W/2) \cdot 3.14$. For each image pair, the real-time elastogram–to-sonogram tumor area ratio and the visual criteria scores were evaluated and the results were averaged point by point.

RF Image Acquisition and Off-line Strain Image Reconstruction

After real-time elastography was performed, for each examined lesion a new

TABLE 1
Explanation of Lesion Scores Assigned at Qualitative Analysis of US Thyroid Elastograms

Image Score	Lesion Visualization	Relative Brightness of Lesion	Regularity of Lesion Margin	Definition of Lesion Margin
1	Not visible	Very dark	Very irregular	Indistinct
2	Barely visible	Markedly darker than surrounding parenchyma	Irregular	Less than 50% of margin distinct
3	Partially visible	Slightly darker than surrounding parenchyma	Moderately irregular	Greater than 50% of margin distinct
4	Very visible	Equally as bright as or brighter than surrounding parenchyma	Regular	Sharp

set of RF echo data that yielded a total of 26 images was acquired during one compression cycle. Digitized frames of in-phase and quadrature echo data consisting of 312 sample sequences (each sequence was an A line separated by a 0.12-mm transducer pitch) were recorded at 16 frames per second and stored in the system memory of the US scanner. The RF signals were initially digitized at 36 Msamples per second, demodulated, and decimated by a factor of two to yield in-phase and quadrature data for electronic transfer and storage. Then, the in-phase and quadrature data were upsampled by a factor of four and remodulated to form RF data for off-line processing.

Elastograms were constructed from correlation-based displacement estimates by using cross-correlation algorithms (14,15). Local displacements are first determined from pairs of sequential RF data frames acquired from the same region in the object at two stages of deformation. Displacements are estimated at two resolutions: first by using a coarse two-dimensional companding method based on the sum-absolute-difference search algorithm and then by using a one-dimensional correlation analysis at a finer resolution. With the two-dimensional companding step, one records the coarse displacements while compensating for unwanted lateral motion by warping the image for the following correlation step. One-dimensional correlation analysis is performed at multiple windows along each segment of the RF data, with quadratic interpolation used for subsample displacement estimation. The local strain information is then calculated as a derivative of the displacements. In the current study, 26 successive frames were taken for each nodule, and 25 displacement elastograms were constructed by comparing the neighboring frames. The derivative of each displacement image was calculated to be the elastogram. After processing, a mean off-line elastogram was formed by averaging 25 images in the strain series. Averaging reduces the strain noise on off-line elastograms while increasing the contrast between soft and hard tissues. This process does not reduce spatial resolution because each image in the series is spatially registered.

The off-line elastograms were evaluated by using the same visual criteria that were used to evaluate the real-time elastograms (Table 1). The elastogram-to-sonogram tumor area ratios for all nodules were calculated by using the methods described earlier. In addition, thyroid gland and thyroid tumor strains were measured in each region of interest placed on the same off-line processed elastogram within the normal thyroid gland adjacent to the tumor and over the tumor area, and the thyroid-to-tumor strain ratio (strain index) was calculated. The sizes of the regions of interest within the normal thyroid glands ranged from 5 to 10 mm. To avoid stress decay over the examination depth, the region of interest within the normal thyroid gland was placed at a depth similar to the depth at which the tumor region of interest was placed. The difference in region-of-interest depth between the tumor and the adjacent normal thyroid gland tissue never exceeded 10 mm.

Biomechanical Testing of Thyroid Gland Tissue Samples

To validate the results of thyroid strain imaging, we performed biomechanical tests on samples of resected tumors and normal thyroid gland tissue by using the EZ-Test mechanical analyzer, which is equipped with a load cell (Interface, Scottsdale, Ariz) rated to 10 N with a resolution of 0.02 N. The experimental geometry was modeled as a uniform applied load acting over the boundary of a semi-infinite elastic solid object (16). The examined tissue samples were assumed to be elastic. The applied stress field was comparable to that used for mechanical measurements of breast tissue (17). Samples were tested with precompression strains of 5%; the diameter of the compressor used was 5 mm, and the applied strain was 10%. During compression, the load and the maximum displacement into the surface of the tissue were continuously recorded. These data were used in the following equation to determine the elastic modulus of the tested specimens (18):

$$E = \frac{2(1 - \nu^2) \cdot qa}{w},$$

where E is the elastic modulus, in kilopascals; ν is the Poisson ratio and equals 0.495; q is the load, in kilopascals; a is the radius of the loaded area, in millimeters; and w is the maximum displacement in the direction of the load, in millimeters.

The time between surgical removal of the tissue and mechanical testing did not exceed 3 hours. Tissue was refrigerated after being removed until the testing was started. From the time of excision to the completion of testing, the moisture content of the tissue was maintained with isotonic saline. The tissue samples were tested at room temperature (24°–26°C) because in a previous study conducted by Krouskop et al, there was an absence of detectable differences in the elastic properties of soft-tissue samples tested at room (24°C) and body (37°C) temperatures (17).

A tissue sample size that ensured that assumptions of homogeneity and isotropy could be justified was selected. Each tissue sample was cut into cylindrical slabs with a height-to-diameter ratio no larger than 1:4. This shape prevented the tissue samples from buckling during compression. To avoid tissue sliding, the diameter of the sample was at least four times larger than the diameter of the compressing indenter (5 mm). Therefore, all lesions smaller than 20 mm were excluded from biomechanical measurements. All biomechanically tested samples were histopathologically examined

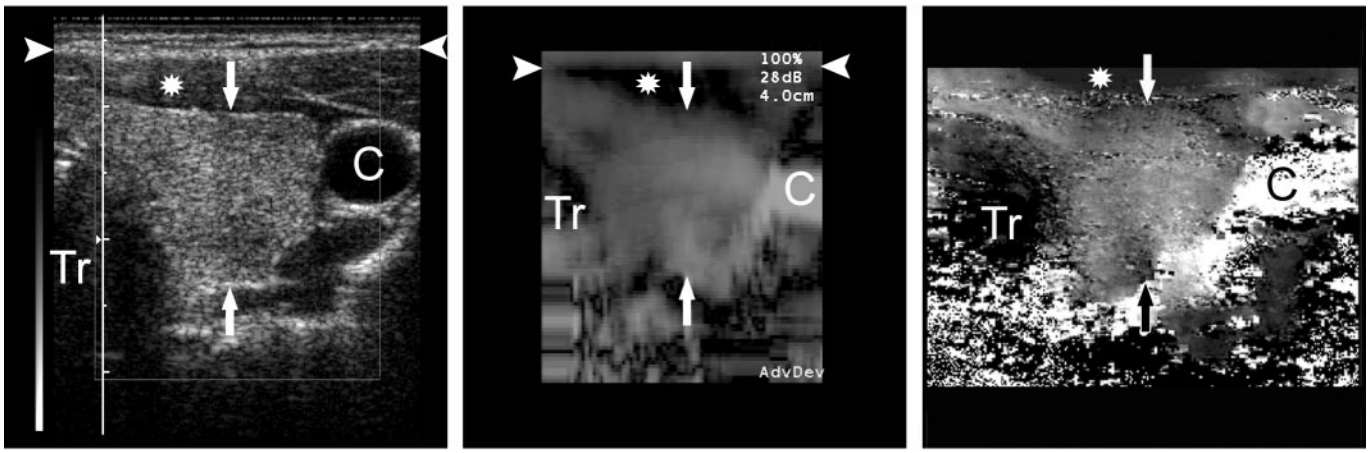

a. b. c.

Figure 1. **(a)** Transverse B-mode sonogram, **(b)** real-time elastogram, and **(c)** off-line processed elastogram obtained in 31-year-old man show a normal left thyroid gland lobe without lesions. Anterior and posterior borders (arrows) of thyroid gland, subcutaneous fat (arrowheads in **a** and **b**), anterior neck muscles (*), carotid artery *(C),* and trachea *(Tr)* are seen.

to confirm the benign or malignant character of the tissue.

Statistical Analyses

Quantitative variables were compared by using the Mann-Whitney *U* test. Qualitative variables were compared by using the χ^2 test. The elastographic characteristics of each thyroid gland nodule were registered separately and processed blindly for statistical evaluation. The unit of analysis was each nodule rather than each patient. One-way analysis of variance was performed to assess differences in the elastographic appearance of lesions between the real-time and off-line processed elastograms, as well as differences in elastographic characteristics between malignant and benign thyroid gland tumors. Forward stepwise multivariate logistic regression analysis was performed to select the variables (among the examined elastographic criteria) that were independently associated with thyroid gland cancer. Each qualitative variable had a binary value—that is, the variable was observed or not observed. Only those independent variables that were found to have statistical significance at $P < .2$ were included in the final multiple logistic regression model. This analysis was performed for real-time and off-line elastography separately.

The sensitivity and specificity of each elastographic criterion included in the final multiple logistic regression model for the differentiation between benign and malignant lesions were calculated by using standard procedures. Correlations between the results of elastographic strain estimation and the results of biomechanical measurements of the examined tissue samples were assessed by using Spearman rank order correlation coefficients (*R* values). Quantitative data are presented as means ± 1 standard deviation. $P < .05$ was considered to indicate significance. Statistical analyses were performed by using a statistical software package (StatView, version 5.0; SAS Institute, Cary, NC).

A post hoc power analysis was performed by using the Fisher exact test for binomial distributions to determine whether the resultant sample size was of sufficient magnitude to yield confidence in the outcome results (19). This power analysis was performed by using another statistical software package (nQuery Advisor, version 4.0; Statistical Solutions, Cork, Ireland).

RESULTS

Normal Thyroid Gland Tissue

Real-time (elasticity imaging mode) elastography.—The thyroid gland in all examined patients was visualized with real-time elastography (Fig 1). Image quality often was compromised by decorrelation artifacts caused by carotid artery pulsation and the nonaxial and out-of-plane movements of the thyroid gland under compression. Subcutaneous fat appeared as a very bright (soft) band in the upper part of the elastogram and was markedly different from the underlying muscles, which were much darker (harder). The anterior, posterior, and medial surfaces of the thyroid gland were easily distinguishable from the surrounding structures in most cases. However, the tissue along the lateral margin of the thyroid gland was almost always obscured by motion artifacts caused by pulsation of the carotid artery. The lower 10–15 mm of the elastogram was not clearly seen because of a substantial amount of noise due to the low signal amplitude at this depth.

Off-line processed elastography.—The off-line processed elastograms of the normal thyroid gland were characterized by higher contrast resolution and somewhat lower spatial resolution (Fig 1). This was because the correlation window used to process the off-line-mode elastograms was larger than that used to process the real-time elastograms. Consequently, subcutaneous fat and the upper layers of the anterior neck muscles were not visualized on the off-line processed elastograms. Like the real-time images, the off-line processed images also had substantial amounts of decorrelation noise near the carotid artery and in deeper parts of the image.

Biomechanical testing of thyroid gland samples.—Results of the biomechanical testing of the normal thyroid gland tissue samples were based on the data collected from a total of 21 patients from whom tissue specimens 20 mm or larger were available. The mean elastic modulus for the normal thyroid gland tissue was 12.3 kPa ± 4.8 (range, 5.8–18.7 kPa).

Thyroid Gland Cysts

Real-time (elasticity imaging mode) elastography.—Thyroid gland cysts, especially those in the center of the gland, were easily visualized on the real-time elasto-

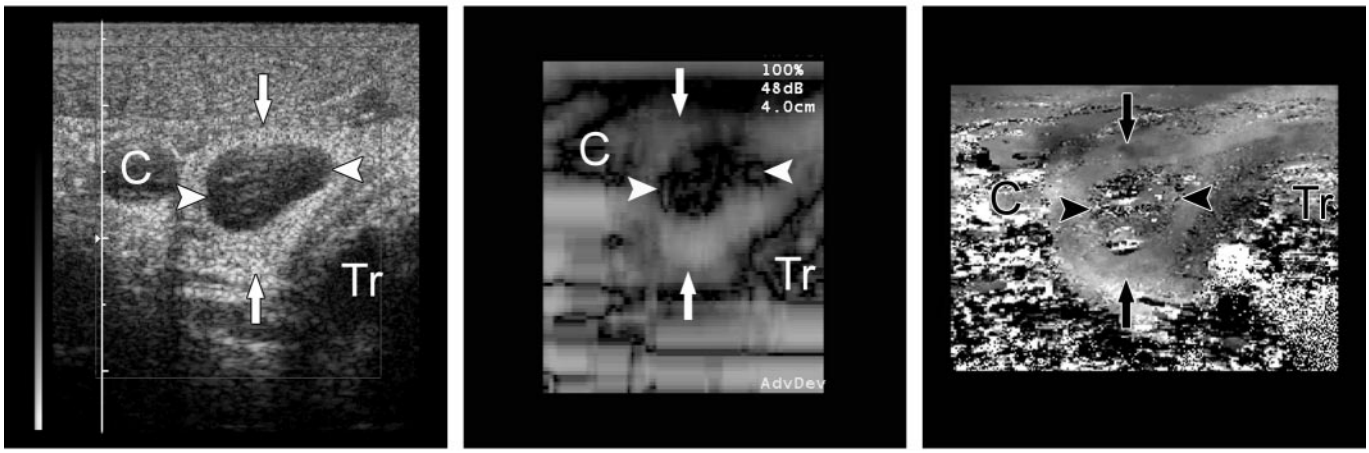

a. b. c.

Figure 2. **(a)** Transverse B-mode sonogram, **(b)** real-time elastogram, and **(c)** off-line processed elastogram obtained in 31-year-old man show a cyst (arrowheads) in the central part of the right lobe of the thyroid gland. In **b**, the cyst is clearly visible as a very dark lesion with a distinct, moderately irregular margin. The off-line processed elastogram (**c**) is characterized by extensive amounts of decorrelation noise in the central area of the lesion due to excessive movements of cyst content under compression. In **a–c**, arrows mark anterior and posterior borders of thyroid gland. *C* = carotid artery, *Tr* = trachea.

TABLE 2
Elastographic Characteristics of Thyroid Nodules

Characteristic	Real-time Elastography*	Off-line Elastography*	*P* Value
Thyroid cysts (n = 6)			
Visualization score	3.12 ± 0.98	3.00 ± 1.09	.8
Relative brightness score	2.83 ± 0.52	2.67 ± 1.03	.5
Margin regularity score	2.58 ± 0.58	2.33 ± 0.82	.7
Margin definition score	2.75 ± 0.99	2.50 ± 1.05	.6
Tumor area ratio	0.89 ± 0.21	0.98 ± 0.41	.6
Solid benign nodules (n = 24)			
Visualization score	2.46 ± 0.61	2.46 ± 0.98	.9
Relative brightness score	2.67 ± 0.82	2.33 ± 0.64	.09
Margin regularity score	2.35 ± 0.71	2.00 ± 0.66	.09
Margin definition score	2.46 ± 0.85	2.25 ± 0.99	.5
Tumor area ratio	0.83 ± 0.18	0.94 ± 0.17	<.01
Strain index	NA	2.11 ± 0.90	NA
Malignant lesions (n = 22)			
Visualization score	2.84 ± 0.60	3.09 ± 0.97	.2
Relative brightness score	2.41 ± 0.88	1.86 ± 0.99	<.05
Margin regularity score	2.27 ± 0.74	2.09 ± 0.87	.6
Margin definition score	2.91 ± 0.67	2.68 ± 1.17	.7
Tumor area ratio	0.94 ± 0.23	1.03 ± 0.16	.3
Strain index	NA	9.82 ± 6.33	NA

Note.—NA = not applicable.
* Data are mean values ± standard deviations.

grams (Fig 2). Three (50%) of the six cysts were highly visible (visualization score > 3), were markedly darker than the surrounding normal thyroid tissue (relative brightness score < 2), and had irregular but distinct margins (margin regularity score < 3, margin definition score ≥ 3). The other cysts were barely or partially visible on the real-time elastograms (visualization score ≤ 3) and were as bright as or slightly darker than the surrounding normal thyroid tissue (relative brightness score ≥ 3). Thyroid gland cysts were significantly smaller on the real-time elastograms than on the corresponding B-mode images ($P < .05$, Mann-Whitney U test); the mean real-time elastogram–to-sonogram tumor area ratio was 0.89 ± 0.21. Mean visual criterion scores are presented in Table 2.

Off-line processed elastography.—The visualization patterns of the thyroid cysts on the off-line elastograms did not differ significantly from the patterns on the real-time elastograms (Fig 2). In contrast to real-time elastograms, the size of the cyst on the off-line processed images and on the corresponding B-mode sonograms did not differ significantly. The mean off-line elastogram–to-sonogram tumor area ratio was 0.98 ± 0.41. On off-line processed elastograms, five (83%) of the six cysts had an extensive amount of noise in the central area of the lesion due to excessive incoherent fluid motion inside the cyst under compression. Therefore, measurements of the nodule strain and calculations of the strain index in the cystic nodules were not performed and these lesions were excluded from analysis of the accuracy of elastographic criteria for thyroid cancer diagnosis.

Solid Benign Thyroid Gland Lesions

Real-time (elasticity imaging mode) elastography.—The majority (n = 21 [88%]) of the solid benign lesions were barely or partially visible on the real-time elastograms (visualization score ≤ 3) (Fig 3). In most cases (n = 21 [88%]), the benign nodules were as bright as or slightly darker than the surrounding normal thyroid tissue (relative brightness score ≥ 3). Only three (12%) of the 24 benign nodules appeared very dark on the real-time elastograms, with relative brightness scores lower than 2. The margins of 21 (88%) benign nodules were classified as irregular (margin regularity score ≤ 3). Moreover, 15 (62%) solid benign lesions had an indistinct margin (margin definition score < 3). In 22 (92%) cases, the

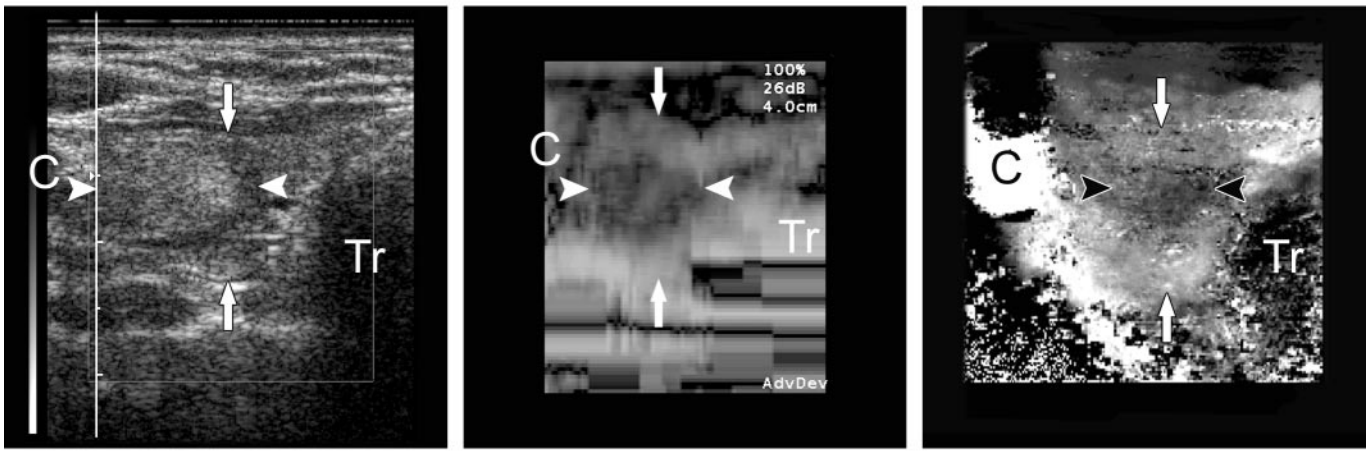

Figure 3. **(a)** Transverse B-mode sonogram, **(b)** real-time elastogram, and **(c)** off-line processed elastogram obtained in 54-year-old woman with a solid benign isoechoic thyroid gland tumor (arrowheads) in the lateral segment of the right thyroid gland lobe. In **b**, the tumor is partially visible; it is markedly darker than the surrounding normal thyroid gland tissue and has an irregular, barely distinct margin. In **c**, the tumor is somewhat visible; it is slightly darker than the surrounding normal thyroid gland tissue and has a very irregular, almost indistinct margin. In **a–c**, arrows mark anterior and posterior borders of thyroid gland. *C* = carotid artery, *Tr* = trachea.

benign nodules appeared smaller on the elastograms than on the corresponding B-mode images. The mean real-time elastogram–to-sonogram tumor area ratio for these lesions was 0.83 ± 0.18.

Off-line processed elastography.—The appearance of the solid benign thyroid lesions on the off-line elastograms was similar to that on the real-time elastograms (Fig 3). The majority (20 [83%]) of the benign nodules were barely or partially visible on the off-line elastograms (visualization score ≤ 3). Almost all (23 [96%]) of the solid benign lesions appeared darker than the surrounding thyroid parenchyma (relative brightness score ≥ 2 but < 4), indicating that the lesions were stiffer than the surrounding tissue. Only one (4%) solid benign lesion was visualized as a very dark focus (relative brightness score < 2). The mean relative brightness score (2.33 ± 0.64) of the lesions on the off-line processed elastograms was slightly lower than that on the real-time elastograms (2.67 ± 0.82; $P = .09$, Mann-Whitney *U* test). The margins of the benign nodules were slightly more irregular on the off-line processed elastograms than they were on the real-time elastograms (mean margin regularity score, 2.00 ± 0.66 vs 2.35 ± 0.71; $P = .09$, Mann-Whitney *U* test).

In contrast to real-time elastograms, the size of benign nodules on the off-line processed elastograms and on the corresponding B-mode sonograms did not differ significantly. The mean off-line elastogram–to-sonogram tumor area ratio (0.94 ± 0.17) was significantly higher than the mean real-time elastogram–to-sonogram ratio (0.83 ± 0.18) ($P < .01$, Mann-Whitney *U* test).

The mean strain of the solid benign lesions measured on the off-line processed elastograms was significantly lower than the strain of the surrounding thyroid parenchyma (2.1% ± 1.8 vs 3.9% ± 4.6; $P < .001$, Mann-Whitney *U* test). The mean value of strain index for these lesions was 2.11 ± 0.90.

Biomechanical testing of solid benign lesion samples.—Results of the biomechanical testing of the solid benign thyroid gland lesion samples were based on the data collected from a total of 13 lesions. Twelve (92%) examined benign lesions were significantly harder than the normal thyroid gland tissue; the mean elastic modulus was 22.5 kPa ± 9.6 (range, 11.9–37.4 kPa; $P < .01$, Mann-Whitney *U* test). The mean benign nodule elastic modulus–to–normal tissue elastic modulus ratio was 2.3 ± 1.7 (range, 0.4–7.3). Neither the solid benign tumor strain index nor the solid benign tumor elastic modulus had a significant correlation with lesion size. On the other hand, the solid benign tumor elastic modulus–to–normal tissue elastic modulus ratio strongly correlated with the strain index ($R = 0.68$, $P < .01$) (Fig 4).

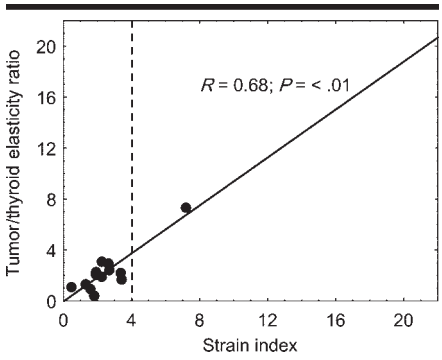

Figure 4. Benign thyroid gland lesion measurements. Graph illustrates correlation between the tumor-to–normal thyroid gland tissue elasticity ratio measured during biomechanical testing of resected thyroid gland specimens and the strain index measured on off-line processed elastograms. There is a significant positive correlation between the relative measurements of benign thyroid gland tumor elasticity evaluated at US elastography and the direct biomechanical measurements used as the reference standard of elasticity in our study. Dashed line represents the threshold strain index value used for the differential diagnosis of thyroid gland cancer.

Thyroid Gland Cancer

Real-time (elasticity imaging mode) elastography.—Thirteen (59%) of the 22 malignant tumors were barely or partially visible on the real-time elastograms (visualization score ≤ 3) (Fig 5). The majority (14 [64%]) of the malignant lesions were darker than the surrounding normal tissue (relative brightness score ≤ 3), and eight (36%) of these lesions appeared very dark on the real-time elastograms (relative brightness score < 2). The margins of 14 (64%) thyroid gland cancers were irregular (margin regularity score ≤ 3). Margins of 16 (73%) malignant tu-

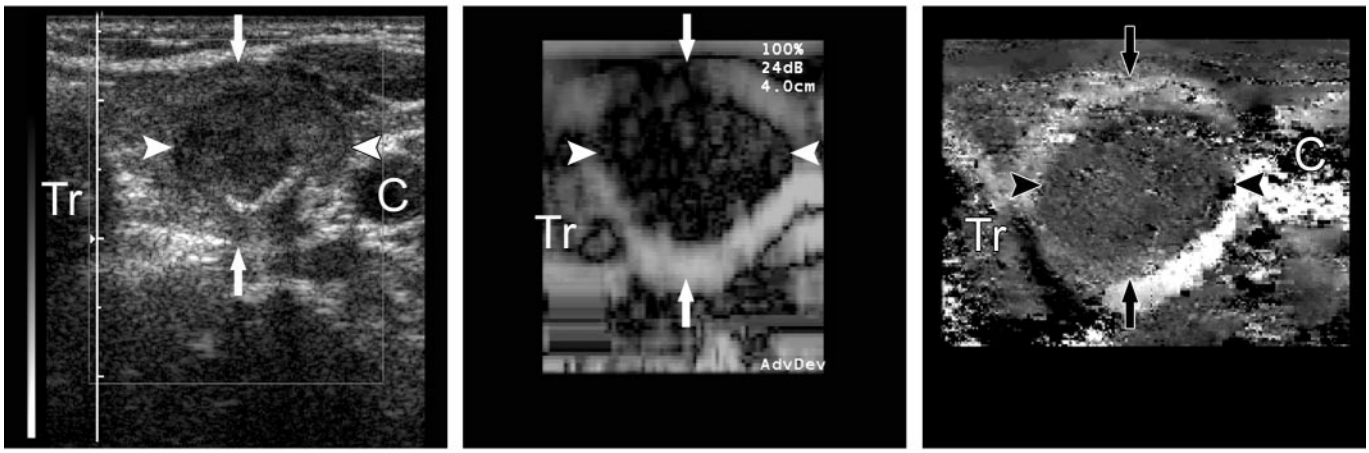

a. b. c.

Figure 5. **(a)** Transverse B-mode sonogram, **(b)** real-time elastogram, and **(c)** off-line processed elastogram obtained in 48-year-old woman with papillary thyroid carcinoma (arrowheads) in the central part of the left thyroid gland lobe. In **b** and **c**, the tumor is highly visible; it is very dark compared with the surrounding normal tissue and has a regular and distinct margin. In **a**–**c**, arrows mark anterior and posterior borders of thyroid gland. *C* = carotid artery, *Tr* = trachea.

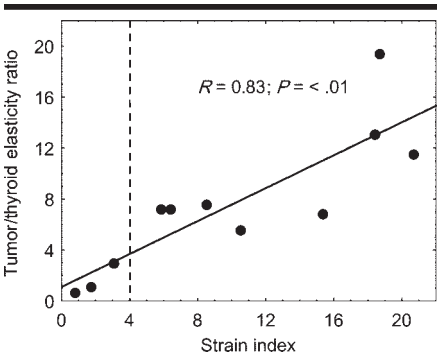

Figure 6. Malignant thyroid gland tumor measurements. Graph shows correlation between the tumor-to–normal thyroid gland tissue elasticity ratio measured during biomechanical testing of resected thyroid gland specimens and the strain index measured on off-line processed elastograms. There is a significant positive correlation between the relative measurements of malignant tumor elasticity evaluated at US elastography and the direct biomechanical measurements used as the reference standard of elasticity in our study. Dashed line represents the threshold strain index value used for the differential diagnosis of thyroid gland cancer.

mors were easily distinguishable from the surrounding tissue (margin definition score ≥ 3). The sizes of the malignant tumors on the real-time elastograms and on the B-mode sonograms did not differ significantly (mean tumor area ratio, 0.94 ± 0.23).

Off-line processed elastography.—Twelve (54%) malignant lesions were clearly visualized (visualization score > 3) (Fig 5) on the off-line elastograms. Twelve (54%) different malignant lesions were darker than the surrounding parenchyma. The other 10 (46%) cancers were slightly darker (relative brightness score < 2). Thus, the mean relative brightness score for the malignant lesions depicted on the off-line processed images (1.86 ± 0.99) was significantly lower than that on the real-time images (2.41 ± 0.88; $P < .05$, Mann-Whitney *U* test). The regularity and definition of the malignant lesion margins depicted on the off-line images were not significantly different from those on the real-time images. The size of malignant lesions on the off-line processed elastograms and on the corresponding B-mode sonograms did not differ significantly (mean tumor area ratio, 1.03 ± 0.16).

Evaluation of the mean strain values for the malignant tumors and the surrounding normal thyroid tissue revealed that all except one of the malignant tumors were much harder than the surrounding parenchyma ($P < .001$, Mann-Whitney *U* test). The mean tumor strain in this group of patients was 0.9% ± 1.1; the mean normal thyroid gland tissue strain, 5.7% ± 6.3; and the mean strain index, 9.82 ± 6.33.

Biomechanical testing of thyroid gland cancer specimens.—Results of the biomechanical testing of the malignant thyroid gland tumors were based on the data collected from a total of 11 lesions. The mean elastic modulus for the cancerous lesions was 99.7 kPa ± 79.8 (range, 15.9–590.4 kPa), which was significantly higher than the elasticity values for the normal tissue and the solid benign lesions ($P < .001$ for both, Mann-Whitney *U* test). One cancer lesion with a substantial amount of central necrosis was softer than the surrounding thyroid gland parenchyma. The mean malignant lesion elastic modulus–to–normal tissue elastic modulus ratio was 8.8 ± 4.6 (range, 0.6–19.4). Neither the strain index nor the elastic modulus of the malignant tumors correlated significantly with lesion size. However, the malignant tumor elastic modulus–to–normal tissue elastic modulus ratio correlated strongly with the strain index ($R = 0.83$, $P < .01$) (Fig 6).

US Elastography in Differential Diagnosis of Thyroid Gland Cancer

Real-time (elasticity imaging mode) elastography.—To evaluate the value of real-time elastography in the differential diagnosis of thyroid cancer, we compared the elastographic appearances of the solid benign and the malignant lesions. Almost half ($n = 9$ [41%]) of the malignant lesions were highly visible on the real-time elastograms and had a visualization score higher than 3. This feature was observed in only three (12%) of the solid benign lesions ($P < .05$, χ^2 test). In addition, a significantly larger proportion of the malignant lesions ($n = 8$ [36%]) appeared very dark on the real-time elastograms; their relative brightness scores were lower than 2 ($P < .05$, χ^2 test). Sixteen (73%) malignant lesions had distinct margins (margin definition score ≥ 3). This feature was observed in only nine (38%) solid benign lesions (χ^2 test, $P < .05$). When we compared the

tumor sizes on the real-time elastograms with those on the corresponding B-mode sonograms, we found that 10 (46%) malignant lesions were larger on the elastograms (tumor area ratio > 1). This feature was observed in only two (8%) of the examined solid benign lesions ($P < .01$, χ^2 test).

Results of multivariate logistic regression analysis (Table 3) showed that only two real-time elastographic criteria—a margin regularity score higher than 3 and a tumor area ratio higher than 1—were significantly associated with thyroid cancer ($P < .05$). These criteria had high specificity (88% and 92%, respectively) but very low sensitivity (36% and 46%, respectively). Other criteria evaluated on the real-time elastograms, such as a tumor visualization score higher than 3 (88% specificity, 41% sensitivity), a relative brightness score lower than 2 (88% specificity, 36% sensitivity), and a margin definition score of 3 or higher (62% specificity, 73% sensitivity), did not have significant associations with thyroid cancer.

Off-line elastography.—The elastographic appearances of the solid benign and the malignant lesions were also compared on the off-line processed strain images. The malignant lesions were much more visible than the benign nodules: 12 (54%) malignant tumors had a visibility score higher than 3. The benign nodules were highly visible on the off-line images in only four (17%) cases ($P < .05$, χ^2 test). Moreover, on the off-line processed elastograms, 10 (46%) malignant lesions and only one (4%) benign one ($P < .01$, χ^2 test) had a very dark appearance (relative brightness score < 2). Distinct borders (margin definition score ≥ 3) were observed in eight (36%) malignant tumors and in only two (8%) benign ones ($P < .05$, χ^2 test). When we compared the tumor sizes on the off-line elastograms with those on the corresponding B-mode sonograms, we found that 12 (54%) malignant lesions were larger on the elastogram than on the corresponding sonogram (tumor area ratio > 1). This feature was observed in only five (21%) examined benign nodules ($P < .05$, χ^2 test). When we compared the strain indexes between the two lesion groups, 18 (82%) malignant tumors and only one (4%) benign tumor were more than four times harder than the surrounding normal tissue (strain index > 4).

Results of multivariate logistic regression analysis (Table 4) showed that only a strain index greater than 4 was strongly associated with thyroid cancer ($P < .001$) at off-line elastography. This criterion had high specificity (96%) and the highest sensitivity (82%) of all the elastographic diagnostic criteria assessed. The false-negative results obtained by using this criterion included two follicular cancer lesions, one very-well-differentiated (grade 1) papillary cancer lesion, and one papillary cancer lesion with a substantial amount of central necrosis and tissue degeneration. There was only one false-positive case with use of this criterion—that of a benign thyroid gland tumor with a substantial amount of calcifications.

Other potential diagnostic criteria that were evaluated on the off-line processed elastograms, such as a tumor visualization score higher than 3 (83% specificity, 46% sensitivity), a relative tumor brightness score lower than 2 (96% specificity, 46% sensitivity), a margin regularity score of 3 or higher (79% specificity, 32% sensitivity), a margin definition score of 3 or higher (92% specificity, 36% sensitivity), and a tumor area ratio higher than 1 (79% specificity, 54% sensitivity), did not have significant associations with thyroid cancer.

TABLE 3
Results of Multivariate Regression Analysis of Elastographic Criteria for Thyroid Cancer Evaluated on Real-time Strain Images

Result	B Coefficient	Standard Error of B	*P* Value
Visualization score > 3	0.17	0.18	.30
Relative brightness score < 2	0.29	0.20	.14
Margin regularity score > 3	0.36	0.17	<.05
Margin definition score ≥ 3	0.15	0.15	.23
Tumor area ratio > 1.0	0.48	0.16	<.05

TABLE 4
Results of Multivariate Regression Analysis of Elastographic Criteria for Thyroid Cancer Evaluated on Off-line Processed Strain Images

Result	B Coefficient	Standard Error of B	*P* Value
Visualization score > 3	0.12	0.15	.43
Relative brightness score < 2	0.05	0.14	.73
Margin regularity score > 3	0.06	0.12	.61
Margin definition score ≥ 3	0.22	0.17	.19
Tumor area ratio > 1.0	0.01	0.12	.9
Thyroid gland–tumor strain ratio > 4.0	0.75	0.13	<.001

Post Hoc Power Analysis

After analyzing the data from this study, we performed a power analysis by using the Fisher exact test to determine whether the resultant lesion sample size was of sufficient magnitude to yield confidence in the outcome results. The estimated proportions were based on the sensitivities of the best real-time (tumor area ratio > 1) and the best off-line (strain index > 4) elastographic criteria for the diagnosis of thyroid gland cancer (46% and 82%, respectively). According to the power analysis results, our sample had a power of 82% for the detection of a difference in sensitivity between real-time elastography and off-line elastography for the diagnosis of thyroid gland cancer at a significance level of 5%. This finding confirmed our initial rationales for selecting the given sample size and study design.

DISCUSSION

US elastography is an imaging modality that has previously been shown to be useful in the differential diagnosis of breast and prostate cancers (10,11). The aims of our prospective study were to evaluate the elastographic appearances of thyroid gland tumors and to determine whether US elastography may assist in the differential diagnosis of thyroid gland cancer. Two different methods of thyroid strain imaging were used in the present study: real-time elastography implemented on a US scanner and off-line processing of strain images reconstructed from RF data stored during US examination.

Real-time strain imaging has some advantages over off-line elastography: First, it is easy to perform and requires no more

than 3–5 minutes of additional examination time. Real-time elastography can be implemented on commercial US systems and used during routine US examinations. In addition, this examination allows the dynamic visualization of tumors during compression.

Off-line processing of strain images involves the use of more sophisticated image-processing algorithms that increase image quality and spatial resolution. In addition, only with off-line processing was it possible to quantitatively measure the stiffness of tissue, compare the stiffness of benign and malignant tumors with the stiffness of the surrounding normal parenchyma, and use the results of these measurements for the differential diagnosis of thyroid cancer. However, this method is more labor intensive and time consuming.

All examined groups of thyroid lesions (ie, cysts and benign and malignant tumors) had different elastographic characteristics. The thyroid cysts were easily visualized on the real-time elastograms as dark lesions with moderately irregular and distinct margins. However, some cysts appeared much brighter, with very irregular and indistinct margins. This may have been owing to possible differences in cyst content (colloid vs hemorrhagic). On the off-line processed elastograms, cysts had similar visibility, but their margins were slightly more irregular and less distinct than they were on the real-time strain images. On the other hand, on the off-line processed elastograms, the cysts were characterized by extensive amounts of noise in the central area of the lesion due to excessive incoherent fluid motion inside the cyst under external compression.

The majority of the solid benign lesions were difficult to see on the real-time elastograms. They had similar brightness or were slightly darker compared with the surrounding normal thyroid gland tissue and had irregular and indistinct margins. The sizes of the benign nodules on the real-time elastograms were significantly smaller than their sizes on the corresponding B-mode sonograms. The margins of these solid nodules on the off-line processed elastograms were less distinct than they were on the real-time elastograms. The sizes of the solid benign lesions depicted on the off-line processed strain images did not differ significantly from the sizes of the solid benign lesions depicted on the corresponding B-mode sonograms.

Malignant tumors were highly visible on the real-time elastograms, and they appeared as dark lesions with irregular and easily distinguishable margins. There was no significant difference between the tumor areas measured on the real-time elastograms and those measured on the corresponding B-mode sonograms. The thyroid gland cancers had similar visibility on the off-line processed and real-time elastograms, but they more often appeared as very dark lesions. The sizes of the malignant tumors depicted on the off-line processed strain images, like the sizes of these lesions on the real-time images, were not significantly different from the sizes of the malignant lesions depicted on the corresponding B-mode sonograms.

In this study, a forward stepwise multivariate logistic regression analysis was performed to select the elastographic criteria that were independently associated with thyroid gland cancer. On the real-time elastograms, only two criteria—a margin regularity score higher than 3 (88% specificity, 36% sensitivity) and a tumor area ratio higher than 1 (92% specificity, 46% sensitivity)—were significantly associated with thyroid gland malignancy ($P < .05$). However, the diagnostic value of these criteria was not high owing to their low sensitivity.

On the off-line processed elastograms, only one criterion—a strain index higher than 4—was shown to be an independent predictor of thyroid gland malignancy ($P < .001$). This criterion had high specificity (96%) and the highest sensitivity (82%) of all the criteria analyzed in this study. The validity of this criterion was confirmed by the results of biomechanical measurements of thyroid gland tissue resected at surgery. These measurements revealed that the malignant tumors were significantly stiffer thyroid gland tissue. The discrepancy in diagnostic performance between the strain index calculations and the observer estimates of relative tumor brightness can be explained by the inadequate sensitivity of the gray map used for elastogram visualization in our study. This map may not have adequately depicted the difference between the hard and very hard lesions, and this limitation may have reduced human observer performance.

There were some limitations in the present study that need to be addressed. Only two cases of follicular thyroid carcinoma were included in the study group, and neither visual analysis nor strain index calculation enabled the differentiation of these tumors from benign thyroid gland nodules. This is because in most cases, the gross anatomy and cellular patterns of follicular carcinoma overlap with those of benign follicular adenoma and this kind of thyroid malignancy can be differentiated from a benign follicular adenoma only when capsular or vascular invasions are discovered at histologic examination.

We can expect elastography to have only limited capability in the differentiation of follicular cancers in its present stage. Because of the design of the current study, we were unable to assess a given observer's ability to diagnose thyroid gland cancer on the basis of elastographic findings. Future studies are required to evaluate the inter- and intraobserver variability and reliability of US elastography for thyroid gland cancer diagnosis.

In general, the diagnostic performance of US elastography will greatly depend on the quality of the freehand compression data acquired and on the specifications of the image reconstruction algorithm used. In our study, the overall quality of both types of strain images (real-time and off-line processed) was significantly affected by decorrelation noise caused by the nonaxial and out-of-plane motion of the examined lesion. In thyroid gland elastography, two main sources of noise can be pinpointed: The first source is pulsation of the carotid artery. We observed a substantial decrease in decorrelation noise on the elastograms of patients who had big thyroid gland nodules, which are not easily affected by carotid artery pulsation. A similar phenomenon was observed on the elastograms of patients in whom the carotid artery was not in direct contact with the thyroid gland.

The second major source of noise is the out-of-plane motion of the examined lesion under compression. The anatomy surrounding the thyroid gland consists of numerous movable structures like the trachea and the jugular vein, so it is difficult to restrict the movement of the thyroid gland to the imaging plane. This problem may be partially solved as the computational capability of US systems increases to a point where we are able to acquire higher-quality primary images at high frame rates.

The quality of elastograms can be improved also by the implementation of new image-processing algorithms based on a regularization of the optical flow constraint (20,21). This regularization method relies on a signal energy minimization approach that is common in the statistical reconstruction algorithms used with other modalities, such as positron

emission tomography and single photon emission computed tomography (22,23). With this application, the energy equation contains a term of echo amplitude conservation, which reflects the basic optical flow constraint, and a regularization term that reduces strain noise by enforcing the spatial smoothness of deformations. However, future prospective study is required to evaluate the clinical usefulness of this method.

In conclusion, elastography is a promising imaging technique that can assist in the differential diagnosis of thyroid cancer. US elastography involving the off-line processing of strain images had higher sensitivity and specificity for thyroid cancer diagnosis compared with real-time elastography. However, the present method of off-line strain image processing is too time consuming and labor intensive for use in busy clinical settings. Future advances in image acquisition and reconstruction algorithms are required to improve the image quality and clinical usefulness of this method.

Acknowledgments: We sincerely thank Siemens Medical Systems, Ultrasound Group, Issaquah, Wash, for technical assistance. In addition, we sincerely appreciate the support of Shimadzu, Kyoto, Japan, in providing a mechanical tester for this study. The authors gratefully acknowledge Junji Konishi, MD, PhD, emeritus professor, Department of Nuclear Medicine and Diagnostic Imaging, Kyoto University Graduate School of Medicine, for his insightful advice and support during the preparation of this study. The authors also gratefully acknowledge Satoshi Teramukai, PhD, assistant professor, Department of Clinical Trial Design and Management, Translational Research Center, Kyoto University Hospital, for his excellent statistical assistance.

References

1. Brander A, Viikinkoski P, Nickels J, Kivisaari L. Thyroid gland: US screening in a random adult population. Radiology 1991;181:683–687.
2. Ezzat S, Sarti DA, Cain DR, Braunstein GD. Thyroid incidentalomas: prevalence by palpation and ultrasonography. Arch Intern Med 1994;154:1838–1840.
3. Watters DA, Ahuja AT, Evans RM, et al. Role of ultrasound in the management of thyroid nodules. Am J Surg 1992;164:654–657.
4. Siperstein AE, Clark OH. Thyroid diseases: tumors, carcinoma of follicular epithelium, surgical therapy. In: Braverman LE, Utiger RD, eds. Werner and Ingbar's the thyroid: a fundamental and clinical text. 8th ed. Philadelphia, Pa: Lippincott Williams & Wilkins, 2000; 898–899.
5. Tan GH, Gharib H, Reading CC. Solitary thyroid nodule: comparison between palpation and ultrasonography. Arch Intern Med 1995;155:2418–2423.
6. Takashima S, Fukuda H, Nomura N, Kishimoto H, Kim T, Kobayashi T. Thyroid nodes: re-evaluation with ultrasound. J Clin Ultrasound 1995;23:179–184.
7. Ross DS. Nonpalpable thyroid nodules: managing an epidemic. J Clin Endocrinol Metab 2002;87:1938–1940.
8. Lerner RM, Huang SR, Parker KJ. Sonoelasticity images derived from ultrasound signals in mechanically vibrated tissues. Ultrasound Med Biol 1990;16:231–239.
9. Ophir J, Alam SK, Garra B, et al. Elastography: ultrasonic estimation and imaging of the elastic properties of tissues. Proc Inst Mech Eng [H] 1999;213:203–233.
10. Garra BS, Cespedes EI, Ophir J, et al. Elastography of breast lesions: initial clinical results. Radiology 1997;202:79–86.
11. Cochlin DL, Ganatra RH, Griffiths DF. Elastography in the detection of prostatic cancer. Clin Radiol 2002;57:1014–1020.
12. Ophir J, Cespedes I, Ponnekanti H, Yazdi Y, Li X. Elastography: a quantitative method for imaging the elasticity of biological tissues. Ultrason Imaging 1991;13:111–134.
13. Chaturvedi P, Insana MF, Hall TJ. Testing the limitations of 2-D companding for strain imaging using phantoms. IEEE Trans Ultrason Ferroelectr Freq Control 1998;45:1022–1031.
14. Chaturvedi P, Insana MF, Hall TJ. 2-D companding for noise reduction in strain imaging. IEEE Trans Ultrason Ferroelectr Freq Control 1998;45:179–191.
15. Pellot-Barakat C, Mai JJ, Kargel C, Herment A, Trummer B, Insana MF. Accelerating ultrasonic strain reconstructions by introducing mechanical constraints. SPIE Med Imaging 2002;4684:323–333.
16. Timoshenko SP, Goodier JN. Theory of elasticity. 3rd ed. New York, NY: McGraw-Hill, 1970.
17. Krouskop TA, Wheeler TM, Kallel F, Garra BS, Hall T. Elastic moduli of breast and prostate tissues under compression. Ultrason Imaging 1998;20:260–274.
18. Lambe TW, Whitman RB. Soil mechanics. New York, NY: Wiley, 1969.
19. Rosner B. Fundamentals of biostatistics. 4th ed. Belmont, Calif: Wadsworth, 1995.
20. Pellot-Barakat C, Frouin F, Insana MF, Herment A. Ultrasound elastography based on multiscale estimations of regularized displacement fields. IEEE Trans Med Imaging 2004;23:153–163.
21. Pellot-Barakat C, Liu J, Frouin F, Herment A, Insana MF. Performance analysis of a regularized algorithm for elasticity imaging. Presented at the IEEE Ultrasonics Symposium, October 5–8, 2003; 1622–1625.
22. de Jong BM, Shipp S, Skidmore B, Frackowiak RS, Zeki S. The cerebral activity related to the visual perception of forward motion in depth. Brain 1994; 117:1039–1054.
23. Noumeir R, Mailloux GE, Lemieux R. Detection of motion during tomographic acquisition by an optical flow algorithm. Comput Biomed Res 1996;29:1–15.